Atmosphere-Ocean
Publication details, including instructions for authors and subscription information:
http://www.tandfonline.com/loi/tato20

Synoptic Climatology of the Southern Beaufort Sea Troposphere with Comparisons to Surface Winds

Matthew G. Asplin[ab], David B. Fissel[a], Tim N. Papakyriakou[b] & David G. Barber[b]

[a] ASL Environmental Sciences Inc., Victoria, British Columbia, Canada

[b] Department of Environment and Geography, Centre for Earth Observation Science, University of Manitoba, Winnipeg, Manitoba, Canada

Published online: 25 Feb 2015.

Synoptic Climatology of the Southern Beaufort Sea Troposphere with Comparisons to Surface Winds

Matthew G. Asplin[1,2,*], David B. Fissel[1], Tim N. Papakyriakou[2] and David G. Barber[2]

[1]*ASL Environmental Sciences Inc., Victoria, British Columbia, Canada*
[2]*Department of Environment and Geography, Centre for Earth Observation Science, University of Manitoba, Winnipeg, Manitoba, Canada*

[Original manuscript received 13 May 2014; accepted 25 December 2014]

ABSTRACT *Synoptic-scale atmospheric circulation patterns drive wind forcing of dynamic and thermodynamic processes in Arctic sea ice. Synoptic typing and compositing are common techniques used to identify a limited number of prevailing weather classifications that govern a region's climate. This work investigates atmospheric circulation patterns (surface to 250 hPa) for the southern Beaufort Sea and corresponding surface wind regimes within each synoptic type. Significant changes* ($p < 0.05$) *in relative frequencies of a number of synoptic types were attributed to declining summer sea ice. Corresponding upper-level circulation anomalies show increasingly meridional atmospheric circulation. Synoptic Types 9 and 11 were identified as key October-November-December circulation features that represent deepening of the Aleutian low with concomitant strengthening of pressure gradients over the southern Beaufort Sea. Classification of coastal-based wind observations shows a shift towards increased easterly wind forcing. A case study of surface wind data from the CCGS* Amundsen *(2009–2011) provided a direct example of the surface wind regime within the marginal ice zone within each synoptic type during a period of reduced Arctic sea-ice cover.*

RÉSUMÉ *[Traduit par la rédaction] Les configurations de circulation atmosphérique d'échelle synoptique guident le forçage par le vent des processus dynamiques et thermodynamiques dans la glace de mer arctique. Le typage synoptique et la composition sont des techniques courantes utilisées pour établir un nombre limité de classifications météorologiques dominantes gouvernant le climat d'une région. Le présent travail examine les configurations de circulation atmosphérique (de la surface à 250 hPa) pour le sud de la mer de Beaufort ainsi que les régimes de vent de surface correspondants à l'intérieur de chaque type synoptique. Les changements significatifs* ($p < 0,05$) *dans la fréquence relative d'un certain nombre de types synoptiques ont été attribués à la diminution de glace de mer en été. Les anomalies correspondantes dans la circulation en altitude font voir une circulation atmosphérique de plus en plus méridienne. Les types synoptiques 9 et 11 ont été identifiés comme des éléments clés de la circulation en octobre-novembre-décembre qui représentent le creusage de la dépression des Aléoutiennes avec le renforcement concomitant des gradients de pression dans le sud de la mer de Beaufort. La classification des observations de vent à partir de la côte montre un déplacement vers un forçage accru par les vents d'est. Une étude de cas de données de vent de surface du NGCC* Amundsen *(2009–2011) a fourni un exemple direct du régime de vent de surface à l'intérieure de la zone de glace marginale dans chaque type synoptique durant une période de couverture de glace de mer arctique réduite.*

KEYWORDS Arctic climate; surface winds; synoptic climatology; synoptic typing; troposphere; Arctic cyclones

1 Introduction

Surface winds are a key environmental physical forcing variable across the ocean–sea-ice–atmosphere interface in the Arctic Ocean. Surface winds transfer momentum to the ocean surface, thus affecting surface ocean currents, ocean turbulence, and sea surface tilt (Guest, Glendening, & Davidson, 1995). Surface winds also transfer momentum to the sea-ice surface, thereby driving sea-ice dynamic processes such as sea-ice drift and ridging of sea ice during the autumn and winter (Rampal, Weiss, & Marsan, 2009; Spreen, Kwok, & Menemenlis, 2011). Persistent winds combined with a large fetch can generate waves with a period and amplitude that increase with the strength and duration of the winds. Large ocean waves and swell may interact with the sea-ice cover, thereby inducing flexural swell within the ice cover (Wadhams, Squire, Goodman, Cowan, & Moore, 1988). Wave forcing of ice may lead to mechanical break-up (Rothrock & Thorndike, 1984), which subsequently exacerbates rates of lateral (Steele, 1992; Curry, Schramm, & Ebert, 1995) and wave-induced melting of ice floes

*Corresponding author's Email: masplin@aslenv.com

(Wadhams, Gill, & Linden, 1979). Furthermore, long waves (swell) can propagate deep within thick, perennial Arctic sea-ice cover (Squire, Vaughan, & Bennetts, 2009) and cause flexural fracture of summer sea-ice cover (Asplin, Galley, Barber, & Prinsenberg, 2012). Depending on the timing, this may serve to enhance lateral melting within the perennial ice cover or merely reduce mean floe size, thereby making extreme multi-year ice (MYI) features, as well as glacial ice features embedded within the pack ice, more mobile (Asplin et al., 2014; Barber et al., 2014). A better understanding of how variability in surface winds affects these coupled processes is critical for developing predictive tools for ice motion, ice management systems, and oil spill trajectory modelling studies.

Sea level pressure gradients, governed by Arctic cyclones and anticyclones drive surface winds over the southern Beaufort and Chukchi seas. The Arctic is widely viewed as a region of cyclolysis for migratory mid-latitude storms. Arctic storms most frequently enter the Arctic from the Barents and Norwegian seas but can also form within the Arctic basin over the Eurasian continent (Sorteberg & Walsh, 2008; Zhang, Walsh, Zhang Bhatt, & Ikeda, 2004). Storms can also enter the Arctic basin from the Pacific Ocean during all seasons; however, friction induced by interaction with topography destroys the necessary back-tilt causing the surface low to fill rapidly. Remnant cyclones that reach the Arctic may reform in a zone of lee cyclogenesis found north of the Alaska Range (Pickart et al., 2009) or the Yukon Mountains (Serreze & Barry, 2005).

Many studies have examined trends in Arctic cyclone frequency, intensity, and origin. Zhang et al. (2004) employed a measure of cyclone intensity, frequency, and duration known as the cyclonic activity index (CAI) to document an increase in the frequency and intensity of storms entering the Arctic from 1979 to 2002, particularly from the North Atlantic and Eurasian sectors of the Arctic. A longer-term study based on cyclonic activity from 1948 to 2002 highlighted an increase in the frequency of incoming Pacific cyclones through Bering Strait and western Canada (Sepp & Jaagus, 2011). Investigation of storm intensities and frequencies from 1981 to 2008 based on a cyclone tracking algorithm showed a shift in cyclone intensities from winter to fall in recent years and a slight increase in cyclone frequencies in spring over the past several decades (Serreze, 2009). Vavrus (2013) identified a small, but significant, trend in the frequency of extreme Arctic cyclones using a historical climate simulation for 1850 to 2005, particularly in sub-polar regions around the Aleutian Islands and Iceland.

Winds are predominantly northwesterly or northeasterly in the southern Beaufort Sea and Chukchi Sea (Maxwell, 1980). Previous studies have attributed westerly winds in the Beaufort Sea to storm activity monitored according to wind intensity and duration thresholds (Hudak & Young, 2002). An assessment of storms from 1979 to 1995 documented frequencies between 6 and 27 storms per storm season (15 June to 15 November) with the highest (lowest) mean monthly storm frequency occurring in October (July) and no significant trend detected in storm frequencies. A more recent study by Barber et al. (2010) similarly reported no trend in storm frequency in the region; however, they suggested that autumn storm intensity may be increasing.

Recent studies have shown that easterly winds over the southern Beaufort Sea have become more frequent and intense during the autumn months of October, November, and December (Moore, 2012; Moore & Pickart, 2012). Extreme wind events (>95th percentile) increased in frequency during all months, with the greatest increases observed in October with 8% more extreme wind events in 2009 compared with 1979 (Stegall & Zhang, 2012). Previous high wind events at Barrow, Alaska, have been documented (Lynch, Cassano, Cassano, & Lestak, 2003; Lynch, Curry, Brunner, & Maslanik, 2004), with strong sustained winds of 25 m s^{-1} observed at Barrow, Alaska, on 3–5 October 1963 and 10–11 August 2000, corresponding with known periods of maximum Arctic cyclone intensity (Hudak & Young, 2002; Serreze & Barrett, 2007; Zhang et al., 2004). Particularly strong northwesterly wind events are noted to be favourable at Tuktoyaktuk, Northwest Territories, during the months of July to September, driven by favourable pressure gradients formed by cyclone-driven cold air pooling behind the Brooks Range in Alaska (Small, Atallah, & Gyakum, 2011). Surface winds are also subject to local enhancement from ice-edge thermodynamic processes (e.g., Hebbinghaus, Schlunzen, & Dierer, 2007).

Synoptic climatology is a powerful analytical branch of climatology for investigating atmosphere–surface interactions (Yarnal, 1985). The classification method employed in the study can greatly affect the nature and number of classifications, thus having a profound effect on the outcome of the study. Synoptic classification schemes vary in sophistication and range from subjective to objective approaches (Frakes & Yarnal, 1997; Yarnal, 1993). Subjective classification requires the researcher to examine the weather charts and assign synoptic classifications manually. This method captures common and important meteorological phenomena; however, it is not easy (even for the original researcher) to reproduce the classifications (Yarnal, 1993). Objective classification methods typically employ statistical methods. Examples of objective classification schemes include the Kirchhofer sum-of-squares (Kirchhofer, 1974), the Lund correlation method (Lund, 1963), principal components analysis (PCA; Yarnal, 1985), self-organizing maps (SOM; Kohonen, 1990), and recursive partitioning (Cannon, Whitfield, & Lord, 2002). These methods can promptly classify large amounts of data with ease; however, they are not completely objective in that they require arbitrary classification thresholds. Slight variations in threshold limits have been shown to significantly alter the number and frequency of synoptic types identified (Frakes & Yarnal, 1997; Key & Crane, 1986). It should also be noted that some statistical methods have been shown to fail outright in some classification schemes, producing random chance classifications that do not represent real meteorological conditions (Blair, 1998).

Hybrid classification schemes that use subjectively selected synoptic "key days" have been found to address the major problems of manual classification (time and inability to replicate the classification) and correlation (threshold limits and arbitrary synoptic type selection; Frakes & Yarnal, 1997). A classification method using a combination of PCA and *k*-means clustering has been employed in numerous studies (e.g., Kidson, 1994; Kidson, 1995; McKendry, Stahl, & Moore, 2006; Stahl, Moore, & McKendry, 2006a, 2006b). Stahl et al. (2006b) emphasized that considerable care should be exercised when selecting the number of clusters so that key circulation features of the meteorology of the region are appropriately captured without duplication.

Sea-ice thickness and volume are notably in decline throughout all regions of the Arctic (Kwok et al., 2009; Laxon et al., 2013; Rothrock, Yu, & Maykut, 1999; Stroeve et al., 2011). The passive microwave satellite record (spanning 1979–2013) shows that summer minimum sea-ice extent in the Arctic is following a linear trend of −7.0% per decade (Stroeve, Markus, Boisvert, Miller, & Barrett, 2014). Arctic surface winds are commonly cited as contributing factors in declining sea-ice thickness and volume (Ogi & Wallace, 2012; Ogi, Yamazaki, & Wallace, 2010), with concomitant increasing regional air temperatures (Overland, 2009), increasing summer ocean mixed-layer temperatures (Perovich, Richter-Menge, Jones, & Light, 2008), and abnormal summer storm activity (Screen, Simmonds, & Keay, 2011). The substantial decline in MYI (Maslanik, Stroeve, Fowler, & Emery, 2011) is purported to be conducive to an increase in the number and mobility of ice hazards in the southern Beaufort Sea (Barber et al., 2014; Galley, Else, Prinsenberg, & Barber, 2013). As the melt season lengthens (Markus, Stroeve, & Miller, 2009; Stroeve et al., 2014), the effect of open water, thin ice, and sensible heat flux on the atmospheric boundary layer above the Arctic sea ice becomes increasingly important to the intensity of Arctic cyclones (Simmonds & Keay, 2009) and regional air temperature anomalies, particularly in fall (Overland, 2009).

The recent trends in autumn Arctic cyclones and surface winds in concert with declining sea-ice extent raise the question as to whether tropospheric circulation patterns are also changing in the Arctic. Atmospheric dynamic processes in the troposphere are responsible for cyclogenesis, steering storms, and atmospheric stability, all of which drive surface pressure patterns and surface winds. Of particular interest is the noted increase in easterly wind forcing during October, November, and December (OND) over the southern Beaufort Sea (Moore, 2012) and concomitant impacts on sea-ice dynamic and thermodynamic processes (Moore & Pickart, 2012). Atmospheric forcing can be investigated using the techniques of synoptic climatology (Yarnal, 1993). The synoptic climatology of the southern Beaufort Sea has previously been analyzed into 12 synoptic types using PCA and subsequent *k*-means clustering on gridded mean sea level pressure data (Asplin, Lukovich, & Barber, 2009). This synoptic climatology can be extended to cover the 1979–2012 period to investigate the relationship between upper-level circulation characteristics (troughs, ridges, pressure gradient intensity, etc), sea level pressure patterns, surface winds, and declining sea-ice cover with the following research questions:

(i) What are the corresponding tropospheric conditions (surface to 250 hPa) within each synoptic type during OND?
(ii) What are the corresponding surface wind statistics for OND synoptic types?
(iii) What is the nature of the variability of OND surface winds within each synoptic type with respect to rapidly declining summer sea-ice cover and subsequent delays in freeze-up (1979–1998 compared with 1999–2012)?
(iv) What are the characteristics of ship-observed surface winds within each of the 12 synoptic types (case study of ship-observed wind dataset for 2009–2011)?

2 Data and methods

a *Gridded Reanalysis Datasets*

Gridded reanalysis meteorological data products are available from a variety of sources and cover different spatiotemporal periods and resolutions (e.g., Kalnay et al., 1996; Mesinger et al., 2006; Vincent et al., 2012). A product at a coarser spatial scale is preferred for examining spatiotemporal circulation patterns at the synoptic scale (i.e., thousand-kilometre, daily-average scales) with methods of synoptic classification. This ensures that mesoscale weather patterns can be classified reasonably within the capabilities of the classification routines used while retaining synoptic-scale circulation features. Finer resolution reanalysis products are useful for direct comparisons of surface-based observations because they can better represent local-scale features. It should be noted that these data reanalysis products offer similar levels of accuracy for locations in the Arctic, mainly because of the lack of surface data inputs to the system.

Daily gridded mean sea level pressure (MSLP) data from 1979 to 2012 (inclusive) were retrieved from archives maintained by the National Oceanic and Atmospheric Administration-Cooperative Institute for Research in Environmental Sciences (NOAA-CIRES) Climate Diagnostics Center, which originated from the National Centers for Environmental Prediction (NCEP) Reanalysis I Project (Kalnay et al., 1996). The spatial resolution of these data is a 2.5°×2.5° (latitude and longitude) grid, encompassing regions of the Beaufort and Chukchi seas (55°–85°N, 120°–175°W). These boundaries were selected to ensure that the Aleutian low and synoptic-scale meteorological features originating over Eurasia and the North Pacific were encapsulated and also to ensure that large-scale synoptic features driving pressure gradients in the region were adequately captured.

b *Regional Synoptic Climatology*

Synoptic-scale atmospheric circulation patterns, hereafter called "synoptic types," were classified from daily MSLP data, thereby expanding the synoptic catalogue of Asplin et al. (2009) to cover 1979 to 2012. Mean daily synoptic types are shown in Fig. 1. The synoptic types were derived using Synoptic Typer 2.2, an application developed by the Australian Bureau of Meteorology (Dahni & Ebert, 1998). Synoptic Typer 2.2 applies a commonly used pattern recognition scheme comprising PCA and a subsequent *k*-means cluster analysis. Daily grids of MSLP data from 1979 to 2012 (12,054 days) were processed unstandardized to leave seasonal effects intact (i.e., values were allowed to vary with the annual cycle). Seasonality is then reflected by the frequency distribution of synoptic types throughout the annual cycle. Seasonal effects can be removed by expressing the data in terms of standardized anomalies, which were calculated by dividing anomalies by the climatological standard deviation.

The typing algorithm determined the eigenvalues for the daily MSLP grids from the correlation matrix with no rotation applied. The first six eigenvectors explain 89% of the variability and were retained; *k*-means cluster analyses were then performed on the component scores of the retained eigenvectors for 9 to 16 clusters. Cluster distance is the dimensionless difference between a sample (daily calculated component scores) and a cluster centroid. The sample is then assigned to the cluster for which the shortest distance to the cluster centroid is calculated. Possible cluster-count options of 10, 12, and 15 were determined by the presence of inflection points in the cluster distance curve. The cluster distance decreases (increases) as greater (smaller) cluster counts are employed and provides a measure of how closely the actual circulation for each day matches its assigned synoptic type. A 12-cluster solution was chosen as the optimal number for this study based on the inflection point for average cluster homogeneity and the physical representation of the major synoptic circulation features in the region. More discussion is available in Asplin et al. (2009).

For each synoptic type, MSLP composites were calculated for the 1979–2012 period (Fig. 1). Seasonal composites of vector surface winds, sea level pressure, and 850, 500, and 250 hPa geopotential heights were calculated. For this paper,

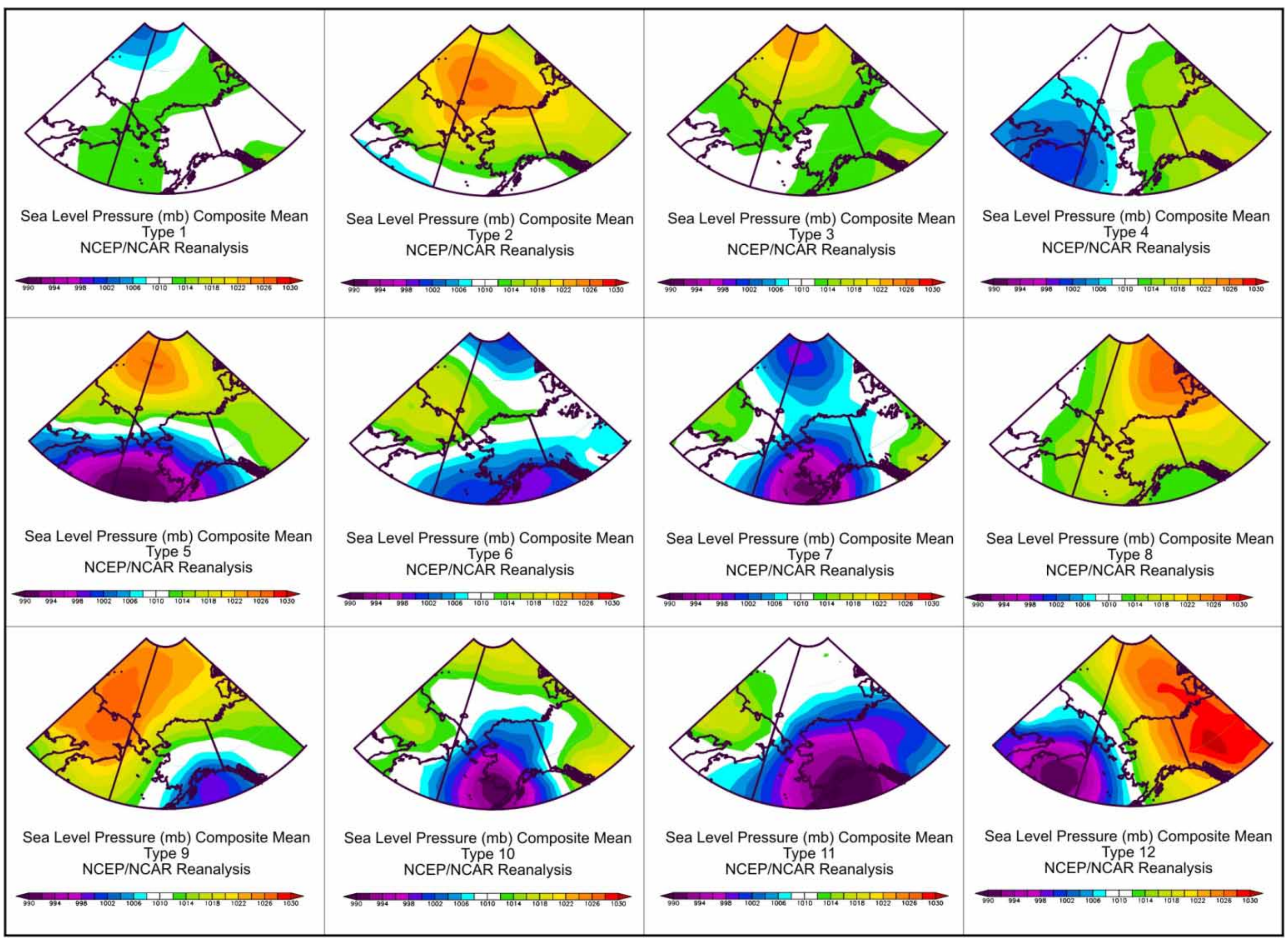

Fig. 1 Mean sea level pressure (hPa) composites for the 12 synoptic types for the analysis period 1979–2012 (adapted from Asplin et al. (2009) with permission of the publisher).

the following seasons were defined: autumn (October to December; OND), winter (January to March; JFM), spring (April to June; AMJ), and summer (July to September; JAS). We focused on OND because this season best represents the freeze-up season immediately following the annual summer minimum Arctic sea-ice extent in September. Mean seasonal composites covering 1979 to 2012 for OND and anomalies from the 1981–2010 climatology were calculated for each synoptic type and tested for significance using a Student's *t*-test.

Synoptic types were divided into two periods, of 10 and 13 years duration each, covering 1979 to 1998 and 1999 to 2012. Changes in seasonal (Table 1) synoptic type frequencies attributed to declining sea-ice extent were assessed using chi-squared frequency analysis by comparing mean synoptic type frequencies for 1999 to 2012 during which declining summer Arctic sea-ice extents were observed to be accelerating compared with those from 1979 to 1998 (Stroeve et al., 2011, 2014). It should be noted that some spatial variability in atmospheric circulation was lost in the daily synoptic classifications because the MSLP composites presented for each synoptic type are averages of sea level pressure (SLP) for all days assigned within each synoptic type (Yarnal, 1993). Furthermore, synoptic type transition (i.e., from one type to the next) cannot be assessed at sub-daily intervals in this study; however, other studies may use sub-daily classification intervals (e.g., 6-hourly).

c *Coastal-based Meteorology*

Hourly wind data are available for Environment Canada weather stations on Pelly Island and at Tuktoyaktuk, Northwest Territories (Fig. 2). The Pelly Island station is an automated weather station reporting basic meteorological variables including wind speed and direction. It is located at approximately 69°36′ N, 135°24′ W in the southern Canadian Beaufort Sea, at an elevation of approximately 12 m above mean sea level. The period of record for wind data is 1995 to 2012. The Tuktoyaktuk station is located at 69°26′ N, 133°01′ W in the southern Canadian Beaufort Sea, at an elevation of approximately 5 m above mean sea level. Wind data are available at this location from 1958 to 2012. These two stations were selected as the coastal measurement locations that best capture the prevailing northwesterly and easterly winds of the region. Stations at Sachs Harbour and Paulatuk, Northwest Territories, were ruled out because of topographic interference with these two key wind directions.

The surface wind data were processed and categorized within each of the 12 synoptic types. Wind data were further subcategorized into two time periods spanning 1979 to 1998 and 1999 to 2012, which represented periods of relatively stable Arctic sea-ice cover and rapidly declining summer sea-ice cover, respectively. It should be noted that the Pelly Island dataset was limited in temporal coverage from 1995 to 2012; hence, the augmentation with wind data from Tuktoyaktuk Airport, which is situated approximately 70 km to the east. Both stations were considered to be in the same geographic region; however, Pelly Island better represents the marine environment.

d *Ship-based Meteorology*

Ship-based data were collected during the ArcticNet–Industry Partnership cruises in the summers of 2009 to 2011. The projects were conducted onboard the research icebreaker CCGS *Amundsen* and summarized in detail in ArcticNet (2014), Asplin et al. (2012, 2014), and Barber et al. (2014). Multidisciplinary sampling was carried out during all three field campaigns with the ship conducting open-water operations in the southern Beaufort Sea within the Pokak and Ajurak oil lease boundaries, along the Beaufort Sea coastline, and throughout the southern Beaufort Sea (Fig. 2).

A meteorology field program was conducted throughout the course of the 2009, 2010, and 2011 research cruises of the CCGS *Amundsen*. Measurements of SLP, air temperature, relative humidity, and wind speed and direction were collected using

TABLE 1. Seasonal percentage synoptic type frequencies: 1979–1998, 1999–2012, and (1999–2012) minus (1979–1998). Significant associations at the 90% and 95% levels are indicated by *($p < 0.1$) or + ($p < 0.05$), respectively.

	Seasonal Frequency (% occurrence)				Seasonal Frequency (% occurrence)				Seasonal Frequency Anomaly (%)			
	Seasonal				Seasonal				Seasonal			
	1979–1998				1999–2012				(1999–2012) minus (1979–1998)			
Synoptic Type	JFM	AMJ	JAS	OND	JFM	AMJ	JAS	OND	JFM	AMJ	JAS	OND
Type 1	5.9	17.2	27.7	8.5	5.2	18.0	31.9	7.4	−0.7	0.8	4.3+	−1.1
Type 2	17.2	12.9	8.2	12.1	16.1	12.8	7.0	10.5	−1.2	−0.1	−1.2	−1.6
Type 3	6.3	14.6	16.1	9.1	7.9	15.3	14.3	7.4	1.6	0.7	−1.8	−1.8
Type 4	5.2	9.3	18.8	6.4	5.0	7.5	17.6	7.3	−0.2	−1.8+	−1.2	0.9
Type 5	12.2	4.9	2.7	13.6	13.2	3.1	2.8	13.5	0.9	−1.8	0.1	−0.2
Type 6	10.7	3.2	6.1	11.6	7.8	3.8	5.9	9.5	−2.9+	0.6	−0.2	−2.0*
Type 7	8.7	4.9	8.6	7.8	8.0	4.5	6.1	6.8	−0.7	−0.5	−2.5*	−1.0
Type 8	3.9	13.2	4.1	3.8	4.5	18.3	5.6	3.9	0.6	5.2+	1.5	0.1
Type 9	9.6	9.3	1.5	4.9	10.4	6.8	0.9	9.0	0.9	−2.5*	−0.6	4.1+
Type 10	7.9	6.2	3.2	7.6	8.9	5.4	2.8	7.9	0.9	−0.7	−0.4	0.3
Type 11	5.2	2.0	2.3	8.5	6.3	1.9	3.4	11.1	1.2	−0.2	1.1	2.6+
Type 12	7.3	2.3	0.8	6.2	6.8	2.5	1.8	5.8	−0.5	0.3	0.9	−0.4

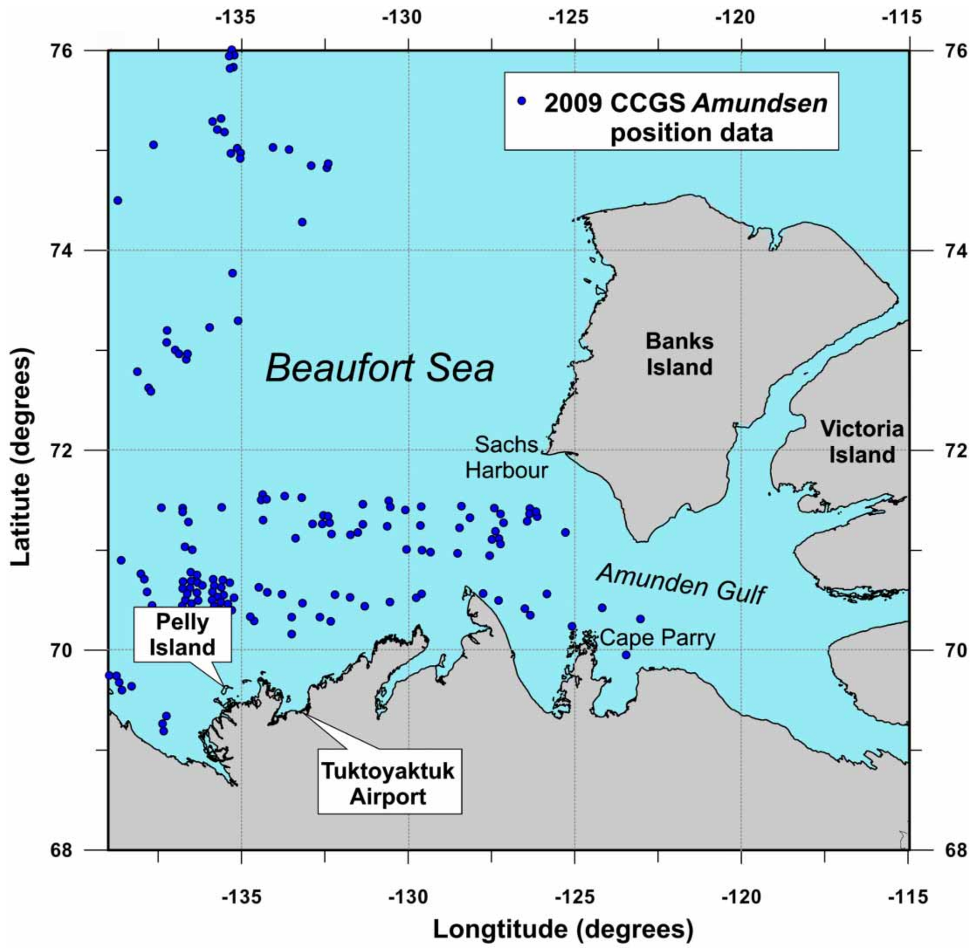

Fig. 2 Southern Beaufort Sea and Environment Canada weather stations. CCGS *Amundsen* 2009 cruise average daily positions are shown from 16 July to 2 November 2009.

an automated weather station located on the foredeck of the CCGS *Amundsen* mounted on an open-lattice tower (Fig. 3). The system obtained atmospheric pressure data using an RM Young 61205 V pressure transducer (0.01 hPa resolution, accuracy of 0.15 hPa). Wind speed and direction were collected using an RM Young 05103 anemometer (directional accuracy of 3°, magnitude accuracy of ±0.6 m s^{-1}). Air temperature and relative humidity were measured with a Vaisala HMP45C212 temperature and relative humidity sensor (temperature accuracy of ±0.1°C and 0–90% relative humidity accuracy of ±2% at 20°C, 90–100% relative humidity accuracy of ±3%). The wind data were filtered to remove periods when eddies from the ship's superstructure may have contaminated the wind data. Further details on the equipment and quality control are available in Else et al. (2011). All meteorological data were scaled to a height of 10 m above mean sea level.

3 Results

a *Synoptic Climatology*

The surface circulation characteristics of the 12 synoptic types of Asplin et al. (2009) were described by MSLP composites (Fig. 1). A detailed discussion of these circulation types is available in Asplin et al. (2009); however, a limited summary is presented for reference in relating their characteristics to the analyses of surface wind data analyses presented in Sections 3b to 3d.

Type 1 was a prominent cyclone type and was observed most frequently during spring and summer (Fig. 1). Types 2 and 3 represented the Beaufort High and occurred frequently throughout the year, although Type 3 had a tendency towards higher mean frequencies during summer. Type 4 showed an SLP dipole pattern that occurred throughout the year, with anticyclonic atmospheric circulation over the Beaufort Sea and early-stage cyclones in the North Pacific resulting in weak, southerly warm air advection from the Pacific into the Arctic. Type 5 occurred most frequently during autumn and winter and represented a strong winter Beaufort High. Types 6 and 7 represented migratory winter cyclones over the Arctic basin (Type 6) and year-round cyclones (Type 7), with both types producing alternating spatial patterns of wind circulation with the passage of cyclones over the study region. Type 8 represented the spring and summer Beaufort High. Types 9 to 11 included a deep Aleutian low that

 http://dx.doi.org/10.1080/07055900.2015.1013438

Fig. 3 CCGS *Amundsen* (left) and foredeck meteorological tower (right). Wind speed and direction were measured at approximately 14.5 m above sea level.

predominated during autumn and winter, driving easterly and southeasterly circulation over the southern Beaufort and Chukchi seas. Type 12 showed a strong SLP dipole pattern, comparable in spatial characteristics to the dipole pattern of Type 4 and occurred most frequently during the autumn and winter. The strong meridional pressure gradient depicted in Type 12 suggests that this synoptic setting may drive strong southerly flows into the Arctic basin. Types 12 and 4 were also representative of the Arctic dipole anomaly, consistent with Wang et al. (2009).

The synoptic climatology was divided into two periods, 1979–1998 and 1999–2012, corresponding to times when summer sea-ice extent was either relatively stable or in rapid decline, respectively. The 12 synoptic types were grouped into four seasonal categories (OND, JFM, AMJ, JAS). Changes in the seasonal percentage frequencies were pronounced (Table 1). Chi-squared frequency analysis revealed that several seasonal synoptic type frequencies were found to vary significantly at the 95% confidence level ($p < 0.05$). The increased frequency (+4.3%) of Type 1 during JAS indicated an increase in summer cyclone activity. Type 8 increased significantly in AMJ ($p < 0.05$), by 5.2%, which represents a stronger spring Beaufort High from 1999 to 2012. Significant ($p < 0.05$) increases in frequency of Types 9 and 11 during OND indicated an increase in easterly wind forcing during the 1999–2012 period associated with the Aleutian low pattern. Types 2 and 3, which were associated with the Beaufort high pressure system, increased non-significantly ($p >$ 0.05) during OND and were noted as possible contributors to easterly and northeasterly wind forcing.

Following documented changes in melt season length (Markus et al., 2009; Stroeve et al., 2014), extreme wind statistics (e.g., Stegall & Zhang, 2012) and increasing OND easterly wind forcing over the southern Beaufort Sea (Barber et al., 2010; Moore, 2012; Moore & Pickart, 2012), we focused on OND months in Sections 3b and 3c with an emphasis on Types 2, 3, 6, 9, and 11. These particular types were selected for further analysis based upon the chi-square frequency analysis presented in Section 3a (Table 1).

b *Upper-level Meteorology (October to December)*

Upper-level tropospheric dynamics are key to governing surface circulation patterns and likely play a role in the observed increase in easterly wind forcing over the southern Beaufort Sea during OND. Mean OND composites covering the 1979–2012 period were generated for surface vector winds, SLP, 850, 500, and 250 hPa geopotential heights were presented for Types 2, 3, 6, 9, and 11 (Fig. 4). Type 2 during OND was characterized by weak surface winds associated with the Beaufort High, with a corresponding high at 850 hPa, and was noted to be linked to an upper-level ridge in the jet stream at 500 and 250 hPa. Type 3 during OND showed a smaller surface high, centred over the Canada Basin, and resulted in strong northeasterly surface winds over the Chukchi Sea. The corresponding upper-level circulation at 850, 500, and 250 hPa suggested this to be a weak surface high, weakly supported by a small upper-level ridge at 250 hPa. The low-pressure feature (cyclone) in Type 6 was supported by an upper-level trough, presenting at 850 and 500 hPa, and a weak trough in the jet stream at 250 hPa. Type 9 yielded moderate northeasterly mean winds, resulting from the interaction of a large ridge of high pressure over Siberia with the Aleutian low and had a a complementary trough at 850 hPa and a distinct meridional circulation pattern in the jet stream at 500 and 250 hPa, featuring a trough over Alaska. Type 11 exhibited a similar surface wind pattern to Type 9, albeit stronger with influence from a

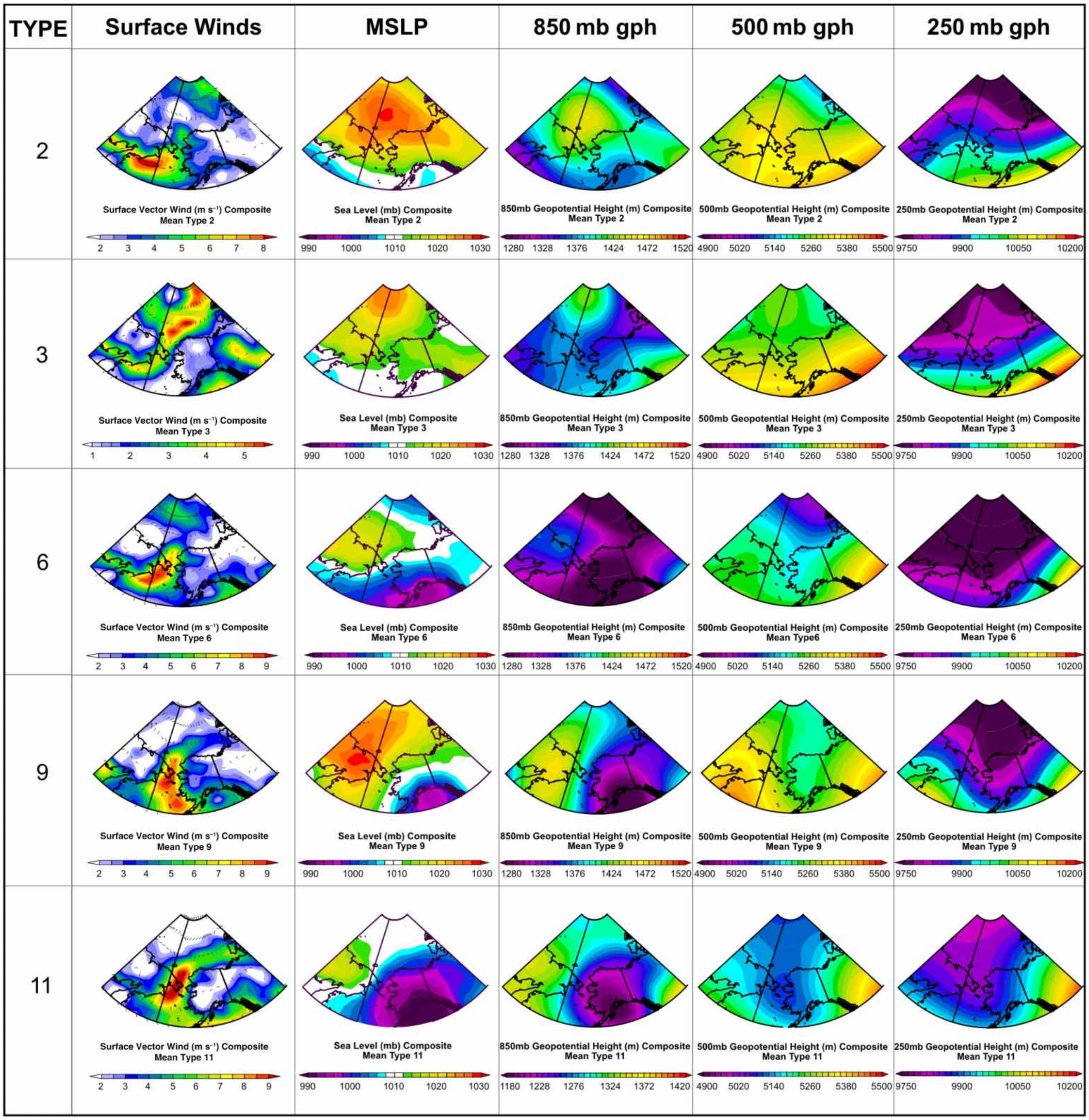

Fig. 4 Mean composites for surface winds, sea level pressure, 850, 500, and 250 hPa geopotential heights for 1979–2012 (October–December).

deep Aleutian low, and was similarly supported by a meridional jet stream.

Anomaly charts for each upper-level variable were computed to investigate any changes in atmospheric circulation during the 1999–2012 period from the 30-year 1998–2010 climatological normals (Fig. 5). Differences were detected for MSLP within all five synoptic types and have corresponding coupled responses in their respective upper-level circulation patterns. Type 2 exhibited a significant ($p <$ 0.05) change in average MSLP of +10 hPa, centred over Bering Strait. This was supported by significant ($p < 0.05$) changes of 60–80 m in geopotential height at 850, 500, and 250 hPa. Type 3 showed a change in MSLP of 4–6 hPa over the Canada Basin and the Aleutian Islands, with similar corresponding significant ($p < 0.05$) changes in geopotential height ranging from 40–80 m detected at 850, 500, and 250 hPa. A change in MSLP over the Canadian Arctic Archipelago (CAA) of −4 hPa was noted with a

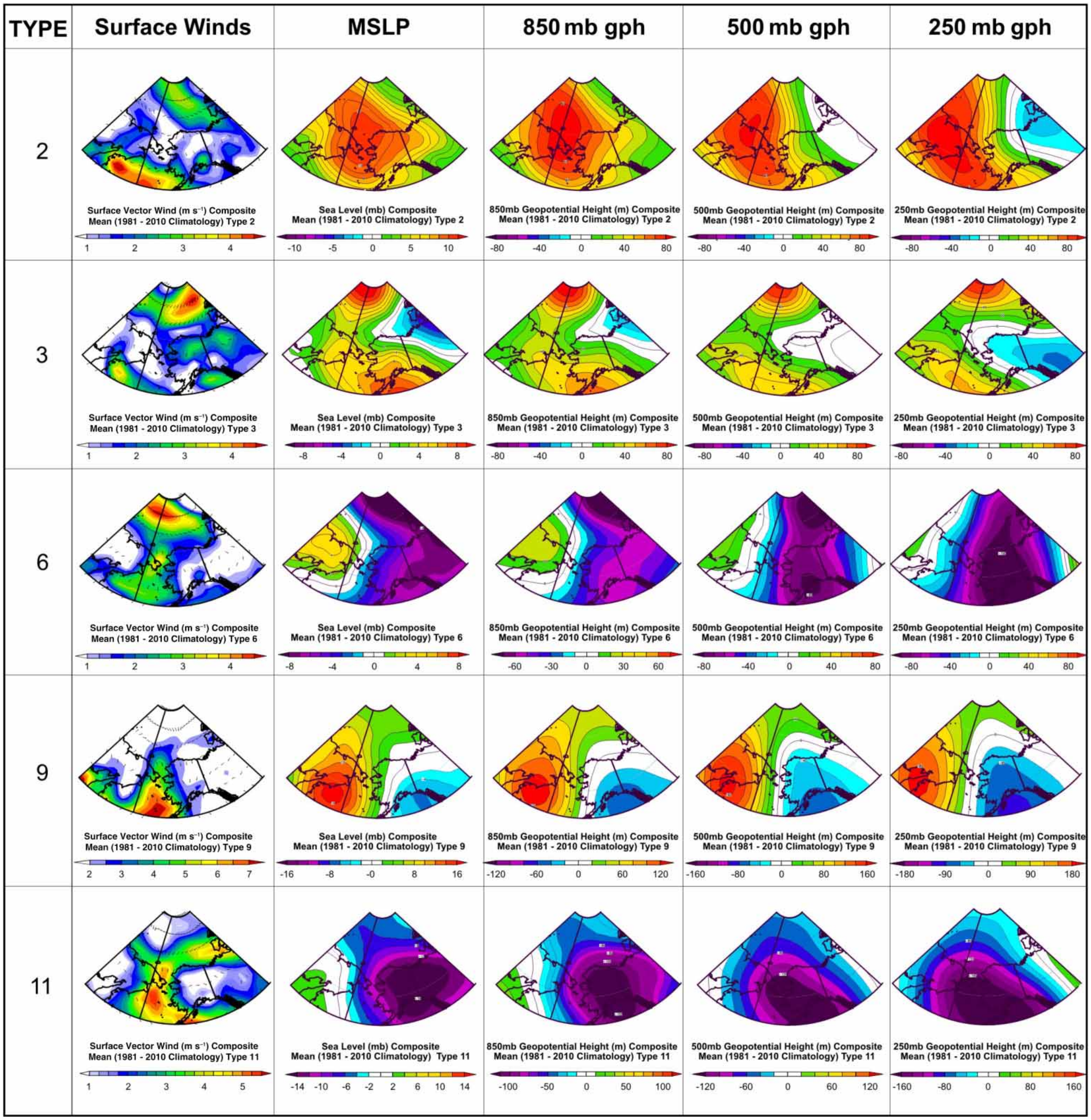

Fig. 5 1999–2012 anomaly from 1981–2010 climatology (October–December). These graphs show how the troposphere (surface to 250 hPa) deviated from the climatological normal during a period corresponding with rapidly declining Arctic summer sea-ice cover and delayed autumn freeze-up.

−40 m change in 250 hPa geopotential height. Type 6 yielded a large, significant ($p < 0.05$) change in MSLP over much of the North American sector in excess of −8 hPa, with a small non-significant variation of 2–4 hPa centred over eastern Siberia. A significant ($p < 0.05$) deep coupled trough was present from 850 to 250 hPa with mean geopotential height deviations ranging from −60 to −80 m.

Types 9 and 11 exhibited the most impressive changes. Type 9 showed a very large significant ($p < 0.05$) strengthening of the high pressure over eastern Siberia by more than 16 hPa, in contrast with the decrease in MSLP centred over the Alaska Panhandle. This represented a strengthening of the pressure gradient in Type 9, thereby driving strong northerly wind anomalies over Bering Strait and moderate easterlies over the Chukchi and Beaufort seas. This pattern occurred

http://dx.doi.org/10.1080/07055900.2015.1013438
Canadian Meteorological and Oceanographic Society

more frequently (4.1%) during OND of 1999 to 2012. Type 11 showed a significant ($p < 0.05$) deepening of the Aleutian low, with the central SLP changing by −14 hPa. Similar to Type 9, this represented a strengthening of the pressure gradient in Type 9; thereby, driving very strong northerly wind anomalies over Bering Strait and strong easterlies over the Chukchi and Beaufort seas. This deepened pattern appears to have occurred more frequently (+2.6%) during OND of 1999 to 2012.

c *Within-Type Variability of Surface Winds (October to December)*

Composites of MSLP for each synoptic type provided a general overview of expected surface circulation patterns; however, surface wind observations are required in order to understand the variability of the speed and direction of surface winds resulting within each synoptic type. Furthermore, the above-noted increased easterly wind forcing during OND was characterized further by within-type investigation of wind directions and intensities between the 1979–1998 and 1999–2012 periods. Wind rose plots were created for analysis of surface wind intensities and frequencies for OND observed at Pelly Island (Figs 6 and 7) and Tuktoyaktuk Airport, Northwest Territories (Figs 8 and 9), for synoptic Types 2, 3, 6, 9, and 11. All five synoptic types captured a surface wind regime described by high frequencies of predominantly easterly, northwesterly, or northerly winds at both locations. Wind intensities tended to range between 0 and 12 m s^{-1}, with extreme cases observed in excess of 24 m s^{-1}, and were comparable to similar extreme wind intensities reported by Stegall and Zhang (2012) for the Alaskan coastal regions.

There were some notable differences in wind direction and intensity statistics within all five synoptic types between 1979–1998 and 1999–2012. Types 2 and 3 exhibited a shift from representing predominantly moderate (6–12 m s^{-1}) easterlies to a bimodal distribution of easterly and northwesterly winds. Wind intensities occasionally exceeded 18 m s^{-1} for both easterly and northwesterly winds in Types 2 and 3, particularly for west-southwest (247.5°) winds in Type 3. Type 6 showed a broadening of representative wind directions ranging from 270° to 100° (northerlies) with an increase in extreme wind values for easterly and northwesterly directions, with intensities occasionally exceeding 12 m s^{-1} and 18 m s^{-1}, respectively. Types 9 and 11 both represented predominantly easterly or east-southeasterly winds during both periods, with the relative frequency of intense wind events increasing for

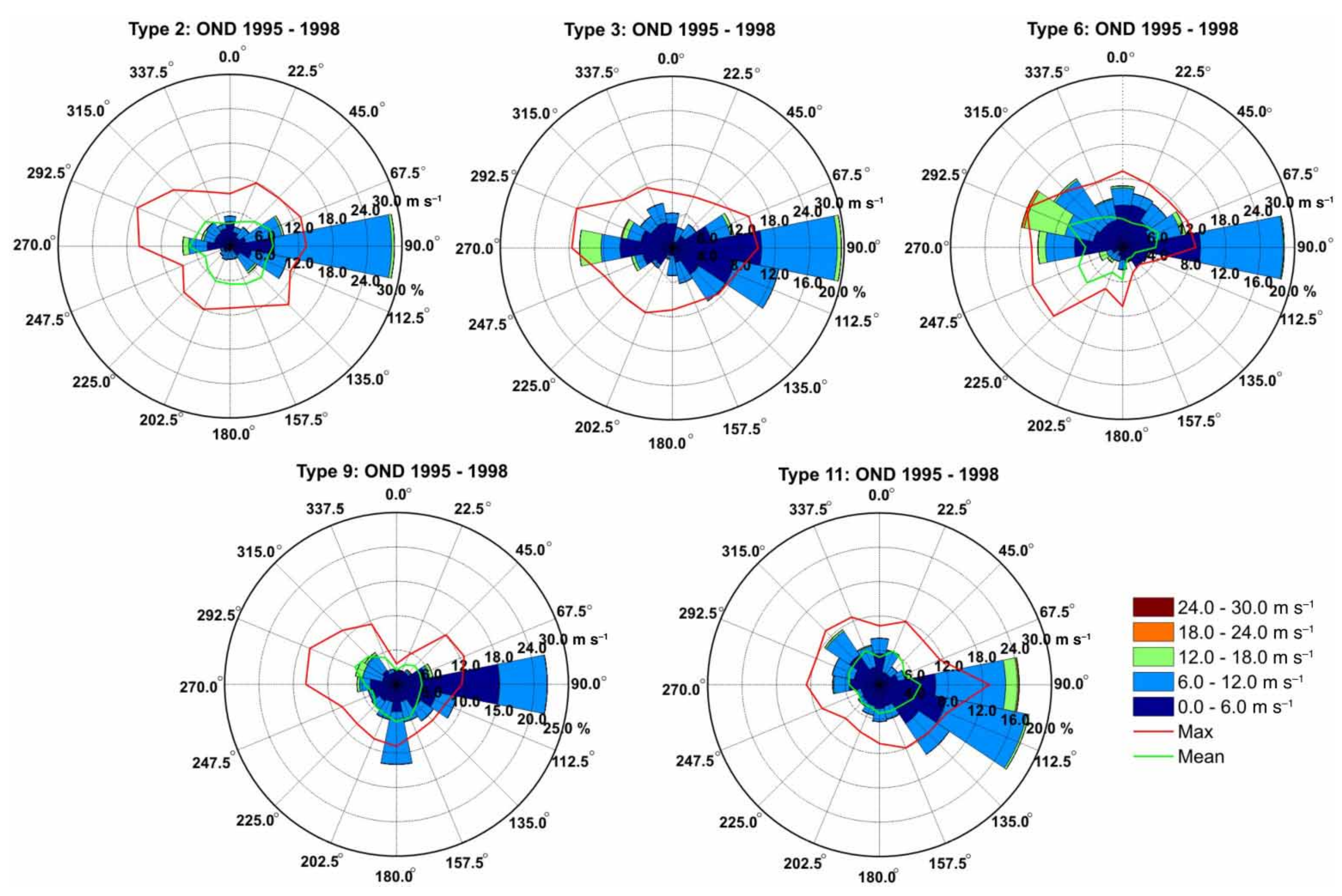

Fig. 6 Surface wind rose plots for 1995–1998 for Pelly Island, Northwest Territories, for synoptic Types 2, 3, 6, 9, and 11 showing relative frequencies and mean and maximum intensities.

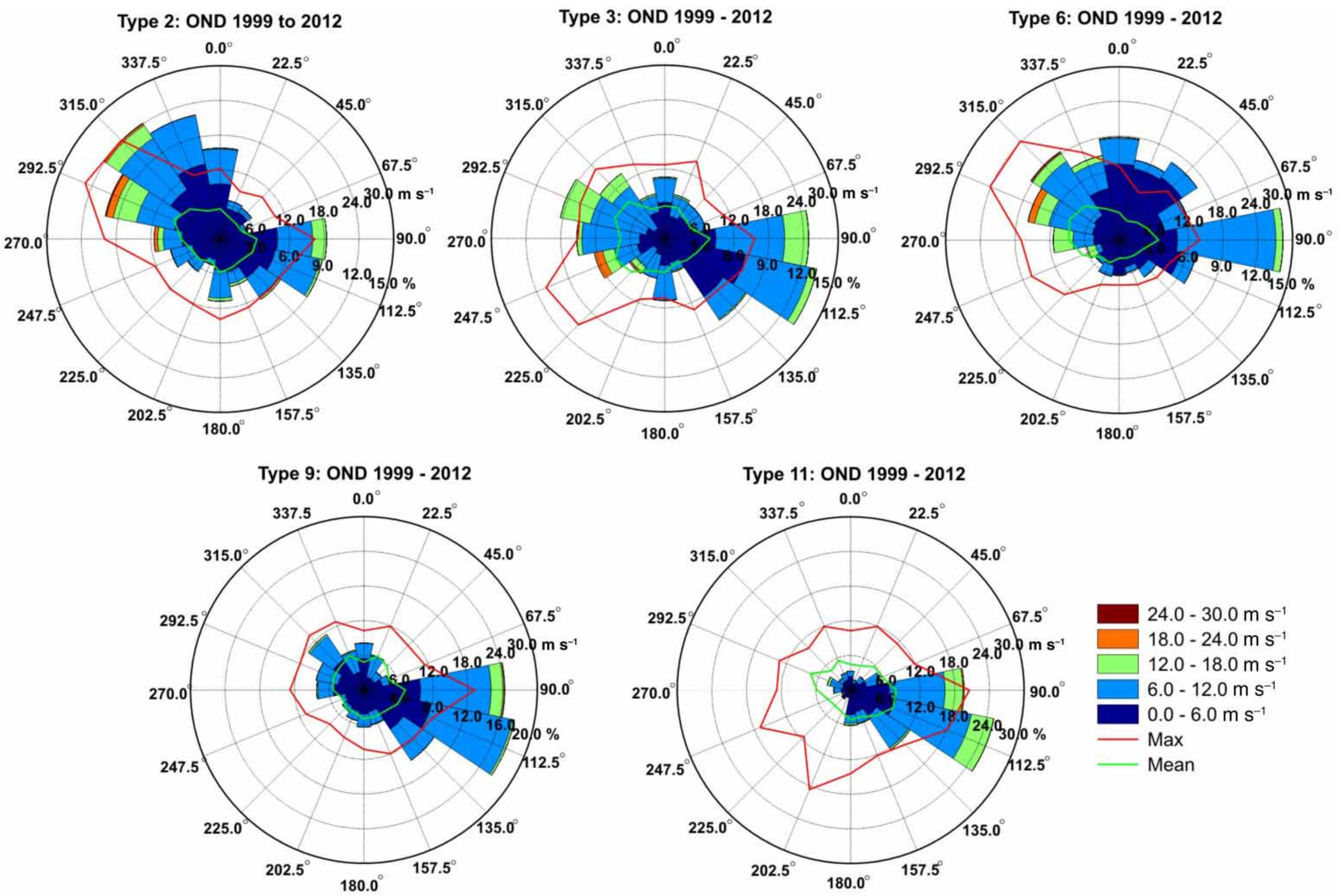

Fig. 7 Surface wind rose plots for 1999–2012 for Pelly Island, Northwest Territories, for synoptic Types 2, 3, 6, 9, and 11 showing relative frequencies and mean and maximum intensities.

both types. Moderate southerly winds (6–12 m s^{-1}) detected for Type 9 during the 1979–1998 period decreased in frequency and intensity and were augmented by a small relative increase in the frequency of moderate northwesterly winds during the 1999–2012 period. Relatively infrequent northwesterly winds detected for Type 11 during the 1979–1998 period appear to decrease to low relative frequencies for the 1999–2012 period.

d *Ship-Based Winds (2009–2011 Case Study)*

Land-based observations were assumed to be representative of surface wind conditions within the marine environment but do not offer the in situ accuracy of ship- or buoy-based wind data. Ship-based observations in this region were extremely limited for the OND period, and the record available tends to follow the late melt season and open-water season (July–October). The CCGS *Amundsen* wind data were classified to characterize within-type surface wind variability for all 12 synoptic types during a period of reduced summer sea-ice cover (2009–2011). All 12 synoptic types were included in this section because of the relatively short period of record for the CCGS *Amundsen* wind dataset. Wind rose plots showed the relative frequencies and intensities of observed surface winds (Fig. 10). Wind intensities were further analyzed with box plots showing the 25th and 75th percentile range, and minimum and maximum observed wind intensities (Table 2) with Types 9, 10, and 12 exhibiting the highest median wind intensities (Fig. 11). There were some constraints with these data, most notably the limited amount of sampling by comparison with coastal wind stations. Furthermore, a spatial constraint existed because of the variability in measurement location (i.e., ship-based measurements). Despite these limitations, the data are valuable because they represent the only in situ source of marine-based measurements. Furthermore, terrestrial measurements of wind speed and direction can be influenced by topography and do not compare well with in situ marine winds (Barber et al., 2014).

Type 1 exhibited a highly variable surface wind regime, with the highest relative frequencies of intense winds occurring for westerly and easterly winds. Type 2 followed a pattern of predominately northwesterly winds, with intensities ranging from weak to intense (>12 m s^{-1}) corresponding with results presented in Section 3c. Although less frequent, the strongest winds measured within Type 2 were westerlies with velocities occasionally exceeding 14.7 m s^{-1}. Type 3 showed a north-northeast wind regime, with northerly

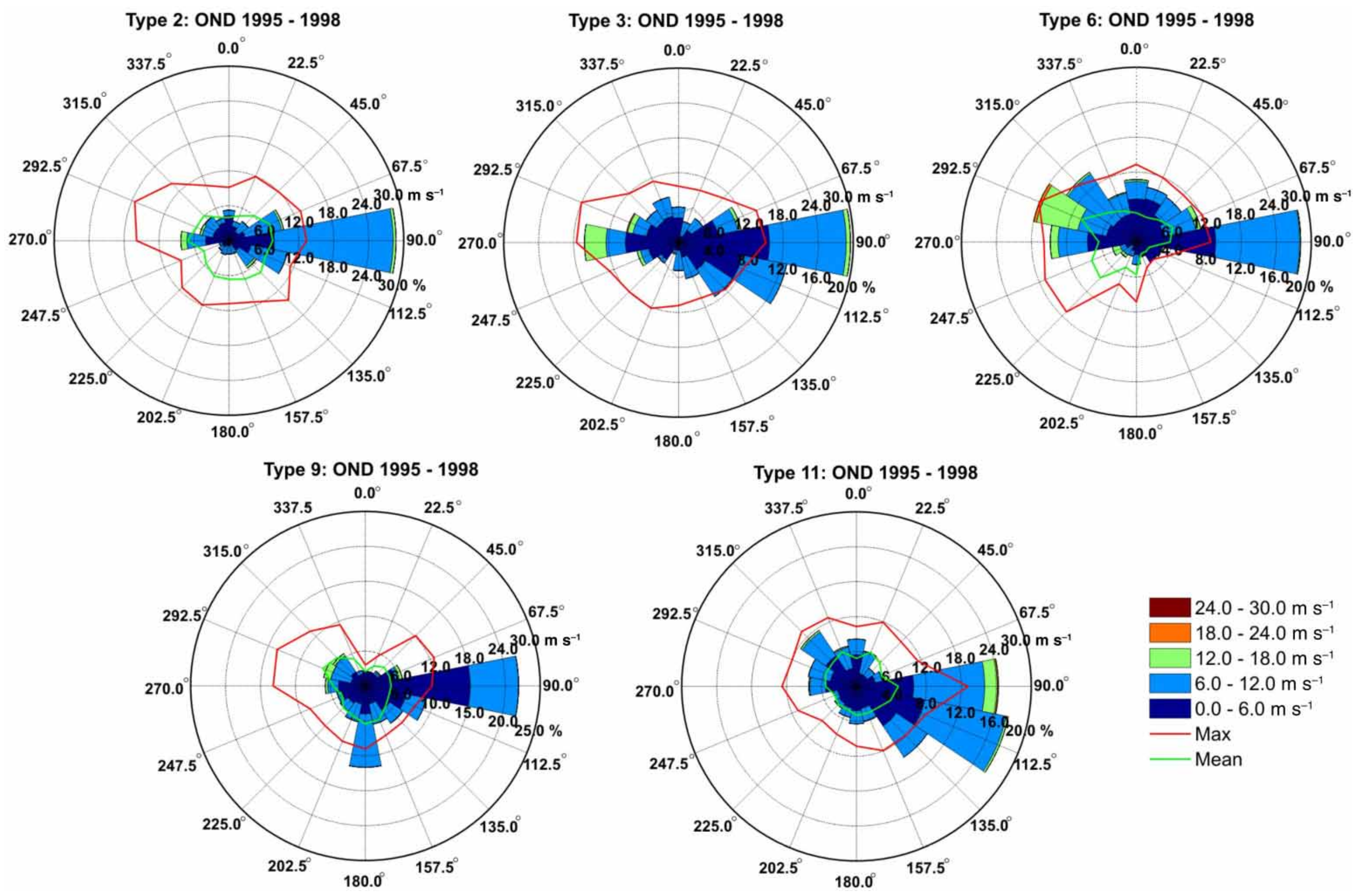

Fig. 8 Surface wind rose plots for 1979–1998 for Tuktoyaktuk, Northwest Territories, for synoptic Types 2, 3, 6, 9, and 11 showing relative frequencies and mean and maximum intensities.

velocities occasionally exceeding 16 m s^{-1}. Type 4 was characterized by a range of wind directions but with easterly winds being the most frequent and intense (10–12 m s^{-1}). Type 5 showed a sharp bimodal distribution of northwesterly and northeasterly winds. The northwesterly winds tended to have moderate intensities (6–10 m s^{-1}), with northeasterly winds occasionally reaching 16 m s^{-1}. Types 6 and 7 both revealed a wind regime similar to Type 1, with highly variable wind directions, with the strongest wind intensities occurring as easterlies or east-southeasterlies. Infrequent intense westerly winds were observed within Type 6. Surface winds for Type 8 were characterized by primarily light northeasterly winds, with very infrequent strong north or northwesterly winds. Type 9 revealed predominant northerlies, with directions ranging from northwesterly to east-southeasterly. Wind intensities varied considerably for northerly winds associated with Type 9 but tended to be consistently strong (10 m s^{-1}) for easterly winds, corresponding with the results of Section 3c. Type 10 reveals a predominantly northeasterly pattern, with occasional frequencies of intense (14–18 m s^{-1}) southerly or southeasterly winds. Type 11 showed wind patterns following either moderate northerly, weak-to-moderate northeasterly, or relatively strong south-southeasterlies. By far the most intense winds associated with Type 11 were southeasterlies, with intensities commonly ranging from 10 to 16 m s^{-1}, corresponding well with results in Section 3c. Type 12 followed a similar wind regime to that observed for Type 11, with a smaller range of wind direction variability.

4 Discussion

The extension of the synoptic catalogue of Asplin et al. (2009) has revealed a number of significant changes in synoptic type frequency by season that may be associated with the declining summer sea-ice cover and delayed freeze-up during OND. These changes were further qualified by examining corresponding anomalies in tropospheric circulation patterns that dynamically affect SLP and atmospheric circulation patterns within each synoptic type. Mean composite geopotential heights for 850, 500, and 250 hPa revealed shifts in circulation that can be linked to observed changes in synoptic type surface circulation characteristics and observations of general northern hemisphere atmospheric circulation change (e.g., Tang, Zhang, & Francis, 2013).

Significant changes ($p < 0.05$) in OND synoptic type frequency were noted for Types 6, 9, and 11 and were concomitant with upper-level geopotential anomalies that suggest increased meridional upper-level flow. This may be linked

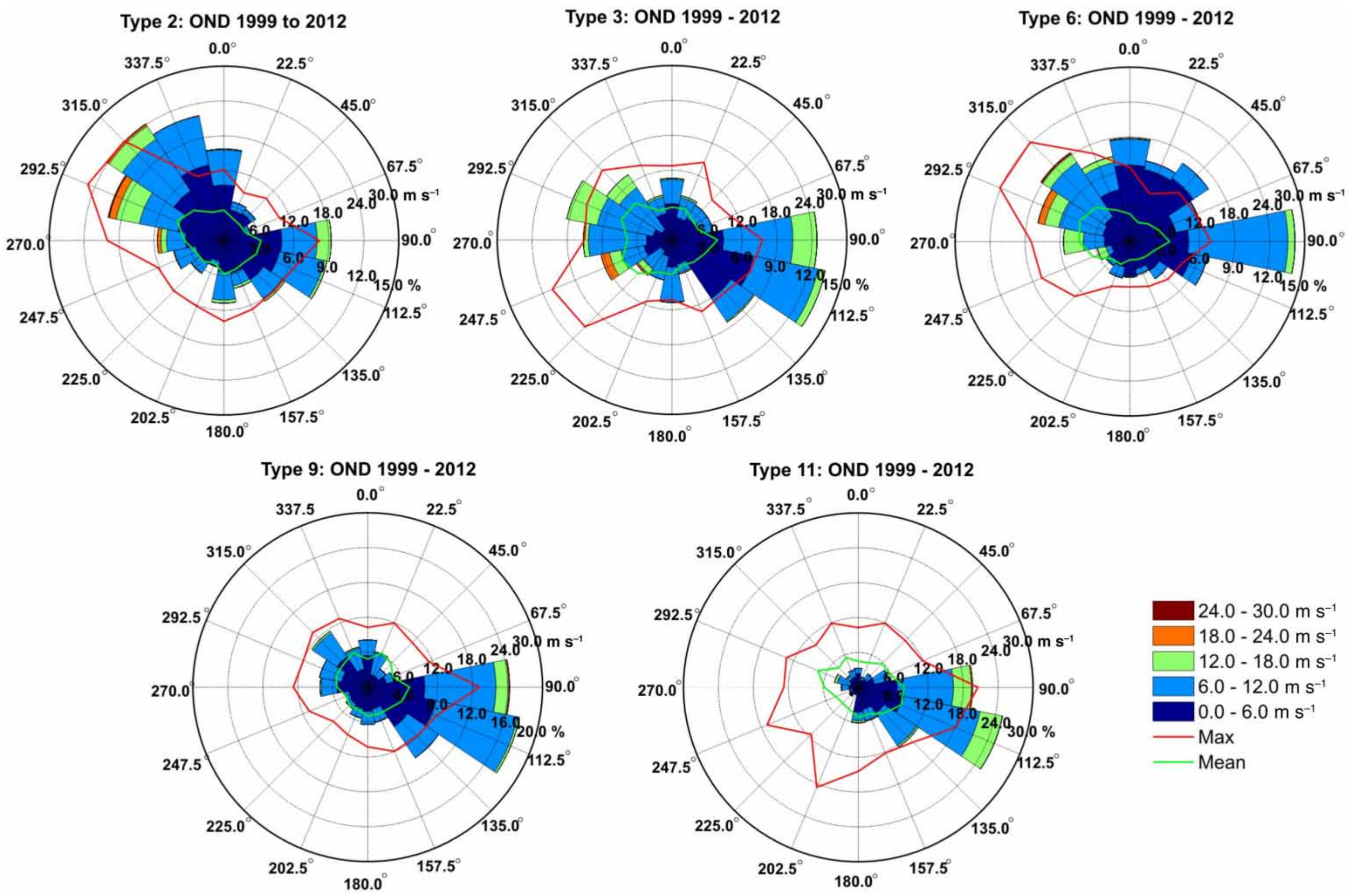

Fig. 9 Surface wind rose plots for 1999–2012 for Tuktoyaktuk, Northwest Territories, for synoptic Types 2, 3, 6, 9, and 11 showing relative frequencies and mean and maximum intensities.

to observations of a meandering polar jet stream in the northern hemisphere (Tang et al., 2013). Type 6 showed a strong meridional shift and deepening of Type 6 cyclones occurring during OND; however, relative frequencies of Type 6 decreased during OND (Table 1). It should be noted that absolute geopotential heights for upper-level circulation in Type 6 tended to be lower because Type 6 has a frequency biased in winter, corresponding with a generally thinner troposphere.

Regional pressure gradients within a select number of synoptic types appeared to be increasing during OND. The increased pressure gradient of Types 9 and 11, coupled with increased relative frequencies of those types, is linked to increases in the frequency of easterly and northeasterly wind events in the Beaufort and Chukchi seas and northerly winds in Bering Strait. Furthermore, the changes detected in the circulation characteristics and frequency of Types 9 and 11 may be linked to recent observations of MYI export through Bering Strait (Babb, Galley, Asplin, Lukovich, & Barber, 2013), driven by a combination of northerly winds and increased sea mobility resulting from declining summer sea-ice cover (Rampal et al., 2009). Increased pressure gradients were detectable in Types 2 and 3, with strengthened and enlarged surface high pressure features. Type 3 showed lower pressure over the CAA, which is likely driving northeasterly wind anomalies over the Chukchi Sea. A stronger north–south pressure gradient was evident in Types 2, 6, and 9. Type 6 exhibited a notable shift in the OND pressure pattern from that of the annual composite (Fig. 1). The Arctic cyclonic circulation feature is shifted onto the Siberian coast and the Aleutian low is shifted to the east. Type 9 shows a deeper Aleutian low during OND, thereby driving stronger northeasterly winds over the Chukchi and Beaufort seas. Average OND composites for Types 2, 3, and 11 exhibited little deviation in the spatial distribution of pressure patterns from the annual average composites.

Classification of surface winds for Pelly Island and Tuktoyaktuk Airport, Northwest Territories, linked changing surface wind climatology to observed changes in the synoptic climatology of the region for OND. The change in surface wind characteristics for Types 2 and 3 at both locations corresponded with strengthening ridges of surface high pressure and concurrent strengthening of pressure gradients over the Beaufort Sea in both types during the 1999–2012 period. These changes, therefore, favoured strong easterly winds over the study region, with occasional shifts to northwesterlies

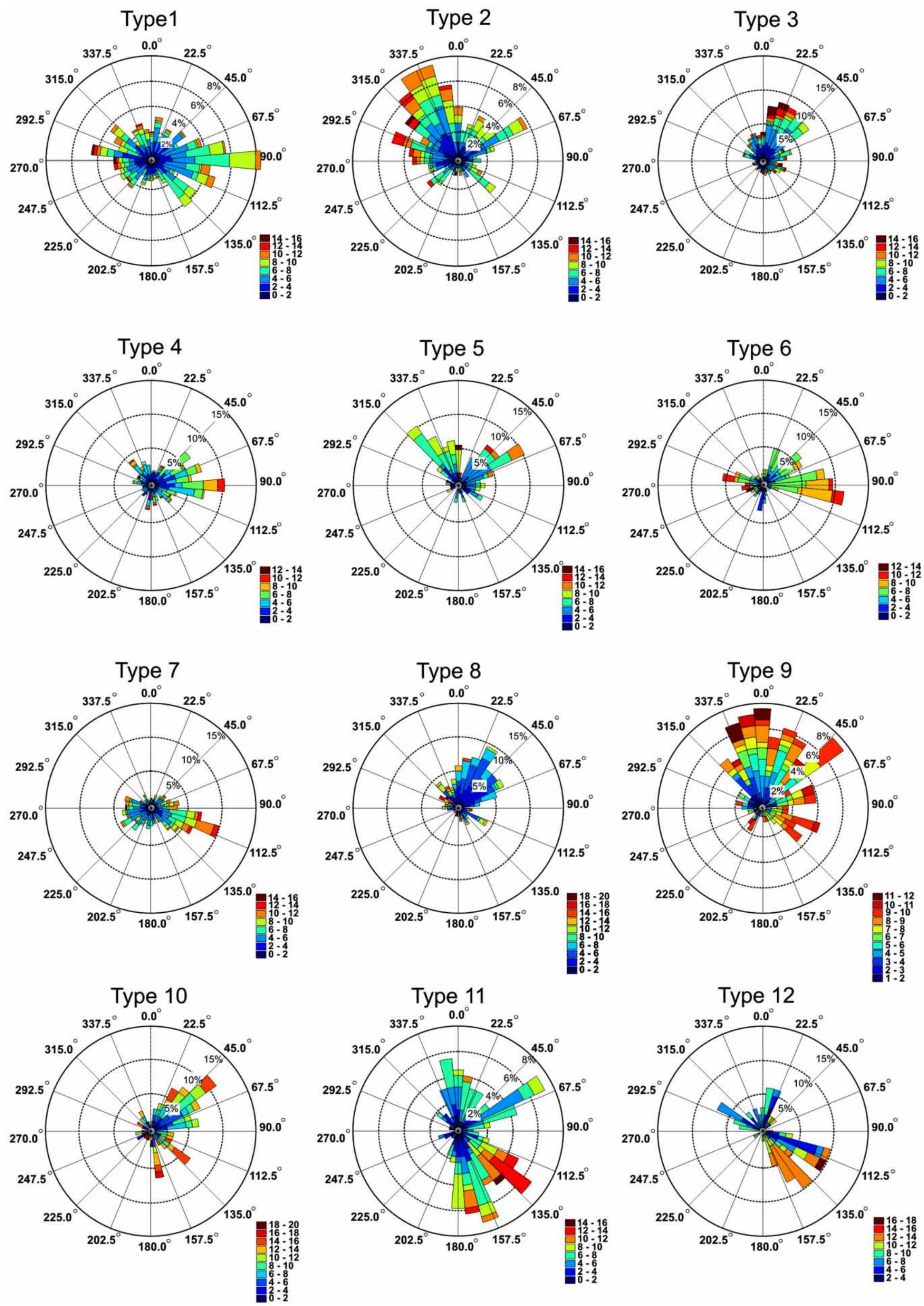

Fig. 10 Hourly averaged surface wind rose plots for CCGS *Amundsen* wind data (2009–2011). Data are categorized by each synoptic type and further subcategorized for wind speed (m s^{-1}) and direction at a 22.5° wind direction interval.

TABLE 2. 2009–2011 CCGS *Amundsen* wind speed (m s^{-1}) summary statistics categorized into the 12 synoptic types (presented graphically in Fig. 11).

	Synoptic Type											
	1	2	3	4	5	6	7	8	9	10	11	12
Min	0.4	0.8	0.7	0.2	1.1	0.9	0.6	0.9	1.0	0.8	0.3	3.5
Q1	5.6	6.0	5.2	4.7	5.8	6.8	5.7	5.0	6.6	8.9	6.1	8.2
Median	3.6	3.8	3.6	3.4	4.3	4.4	4.3	3.4	4.1	5.5	3.5	5.9
Q3	7.4	8.0	7.4	6.4	7.5	7.9	8.1	7.0	8.6	12.8	7.7	11.4
Max	14.6	14.7	15.5	12.8	14.1	12.3	14.3	18.5	11.8	19.1	14.7	16.7
N	735	334	466	479	147	177	409	262	228	108	222	102

corresponding with variability in the location and strength of the surface high represented in both types. Type 6, which represents Arctic cyclones, exhibited a broadening of surface winds during the 1999–2012 period at both sites. The noted increase in variability in wind direction identified within Type 6 is likely attributed to the dipole anomaly in surface to 250 hPa atmospheric circulation patterns, identified in Section 3b. This would correspond with changes in the autumn storm track and intensity associated with delayed freeze-up, following Serreze (2009). Increased frequencies and intensities of easterly wind events in Types 9 and 11 appear to be driven by deepening of the Aleutian low, particularly in Type 11, which is attributable to the meridional jet stream patterns (e.g., Francis & Vavrus, 2012).

The surface wind rose plots generated for wind data from the CCGS *Amundsen* showed that each of the 12 synoptic types had one or two predominant characteristic prevailing wind directions. The two notable exceptions were Type 11, with three predominant directions, and Type 1, with relative frequencies of all wind directions in addition to a predominantly easterly wind regime. The highly variable surface winds in Types 1, 6, and 7 corresponded to their association with cyclone types (Asplin et al., 2009). Types 9 and 11 yielded strong north-northeasterly and southeasterly wind regimes, respectively. This generally followed the observations at the coastal weather stations; however, the spatiotemporal variability in ship location, along with the more limited amount of sampling available, likely introduces bias and a direct comparison must consider the relative location of the ship.

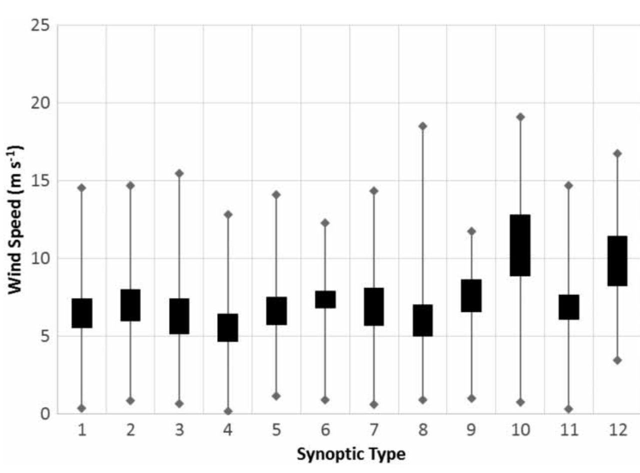

Fig. 11 Box plots of the CCGS *Amundsen* hourly averaged wind speed distribution by synoptic type (2009–2011). The top and bottom of the box indicate the 75th and 25th percentile wind speeds, respectively.

The ship-based surface wind characteristics of each synoptic type, combined with the seasonal occurrence frequencies from 2009 to 2011, were representative of the regional surface wind anomalies relative to the 1981–2010 climatological normals. The net result is enhanced northeasterly and easterly winds, characteristic of the persistent SLP high over the Beaufort and Chukchi seas, that contributed to the record minimum summer sea-ice extent in 2007, in addition to enhanced meridional (south–north) synoptic-scale circulation associated with the Arctic dipole anomaly (Wang et al., 2009; Wu, Wang, & Walsh, 2006). Despite regional differences in relative zonal (east–west) and meridional (north–south) contributions, wind anomalies showed enhanced winds throughout the Beaufort Sea region relative to 1981–2010.

5 Conclusions

This study employed the synoptic climatology of Asplin et al. (2009) to investigate atmospheric circulation patterns in the southern Beaufort Sea by contrasting mean synoptic type frequencies between 1979–1998 and 1999–2012, the latter period representing years of rapidly declining Arctic sea-ice cover and delayed autumn freeze-up. With an emphasis on changing OND synoptic climatology, the overlying upper-level geopotential height patterns were investigated for a select number of synoptic types whose relative frequency was found to vary significantly between 1979–1998 and 1999–2012. Significant changes ($p < 0.05$) in OND synoptic type frequency were found for Types 6, 9, and 11 that are likely caused by increasingly meridional circulation patterns in the northern hemisphere.

Synoptic Types 9 and 11 were identified as key circulation features in the changing regional climate in the southern Beaufort Sea during OND. A combination of increasing relative frequencies of these types and deepening of the Aleutian low, with a concurrent increase in the pressure gradient over the southern Beaufort Sea, were linked to increases in the frequency and intensity of easterly and northeasterly wind events in the Beaufort and Chukchi seas and northerly winds in Bering Strait. Similar responses were detected in Types 2 and 3 for OND, with concomitant increases in strong northwesterly winds for those types with occasional easterlies. These changes all are consistent with observations of increased meridional atmospheric circulation in the northern hemisphere, corresponding with the findings of Francis and Vavrus (2012) and Tang et al. (2013) and may be evidence of increasing Arctic cyclone intensity during the fall, as suggested by Vavrus (2013).

The case study of surface wind data from the CCGS *Amundsen* from 2009 to 2011 provided a direct measurement of the surface wind regime within each synoptic type during a period of reduced Arctic sea-ice cover. This analysis revealed that wind direction and intensity for ship-based observations can be classified within synoptic types, yielding distinct wind direction–intensity regimes within each synoptic type. Types 9 and 11 yielded strong north-northeasterly and south-easterly wind regimes, respectively, and follow the general characteristics of these types at coastal weather stations. Types 1, 6, and 7 showed highly variable wind direction and intensity, corresponding with their previous denotation as Arctic cyclone types by Asplin et al. (2009).

Future work should focus on continued monitoring of surface wind climatology in the southern Beaufort Sea as summer sea-ice extent continues to decline in the Arctic. With recent predictions suggesting that an Arctic melt season resulting in at least one day with a predominantly ice-free Arctic Ocean is now expected between 2020 and 2030 (Overland & Wang, 2013), it is prudent to follow the impacts of reduced summer sea-ice cover, delayed onset of freeze-up, and associated impacts on regional atmospheric circulation. Changes in the surface wind climatology of this region will affect sea-ice dynamic and thermodynamic processes during autumn and early winter, which will subsequently affect industrial activities, transportation, and other activities in the region.

Acknowledgements

Thanks go to the Natural Sciences and Engineering Research Council (NSERC) for an industrial postdoctoral fellowship (IRDF) awarded jointly to M.G. Asplin and ASL Environmental Sciences, Inc., the ArcticNet Network of Centres of Excellence, the Canada Research Chairs (CRC), Canada Foundation for Innovation (CFI), and NSERC Discovery Grants to T.N. Papakyriakou and D.G. Barber. We also acknowledge the Industry–ArcticNet Partnership program with funding for field work coming from BP Canada, Imperial Oil Resources Ventures Ltd. The National Centers for Environmental Prediction (NCEP) provided the reanalysis data, and Environment Canada provided the surface wind data for the southern Beaufort Sea stations. Thanks to Robert Dahni of the Commonwealth Bureau of Meteorology, Melbourne, for permitting us to use Synoptic Typer 2.2. Thanks go to D. Sadowy of ASL for assistance in processing the Environment Canada wind data and R. Bowen of ASL for improving the figures in this manuscript. Special thanks to the captains, officers, and crew of the CCGS *Amundsen* for making the ArcticNet–Industry Partnership field programs a success.

References

ArcticNet. (2014). *Impacts of environmental change in the Canadian Coastal Arctic: A compendium of research conducted during ArcticNet Phase II (2008–2011)*. Québec City, Canada: ArcticNet Inc.

Asplin, M. G., Lukovich, J. V., & Barber, D. G. (2009). Atmospheric forcing of the Beaufort Sea ice gyre: Surface pressure climatology and sea ice motion. *Journal of Geophysical Research Oceans*, *114*, C00A06. doi:10.1029/2008JC005127

Asplin, M. G., Galley, R., Barber, D. G., & Prinsenberg, S. (2012). Fracture of summer perennial sea ice by ocean swell as a result of Arctic storms. *Journal of Geophysical Research Oceans*, *117*, C06025. doi:10.1029/2011JC007221

Asplin, M. G., Scharien, R., Else, B., Howell, S., Barber, D. G., Papakyriakou, T., & Prinsenberg, S. (2014). Implications of fractured Arctic perennial ice cover on thermodynamic and dynamic sea ice processes. *Journal of Geophysical Research Oceans*, *119*, 2327–2342. doi:10.1002/2013JC009557

Babb, D. G., Galley, R. J., Asplin, M. G., Lukovich, J. V., & Barber, D. G. (2013). Multiyear sea ice export through the Bering Strait during winter 2011–2012. *Journal of Geophysical Research Oceans*, *118*, 5489–5503. doi:10.1002/jgrc.20383

Barber, D. G., Asplin, M., Gratton, Y., Lukovich, J., Galley, R., Raddatz, R. L., & Leitch, D. (2010). The international polar year (IPY) Circumpolar flaw lead (CFL) System study: Introduction and physical system. *Atmosphere Ocean*, *48*(4), 225–243. doi:3137/OC317.2010

Barber, D. G., McCullough, G., Babb, D., Komarov, A. S., Candlish, L. M., Lukovich, J. V., … Rysgaard, S. (2014). Climate change and ice hazards in the Beaufort Sea, *Elementa: Science of the Anthropocene*, *2*, 000025. doi:10.12952/journal.elementa.000025

Blair, D. (1998). The Kirchofer technique of synoptic typing revisited. *International Journal of Climatology*, *18*(14), 1625–1635.

Cannon, A. J., Whitfield, P. H., & Lord, E. R. (2002). Synoptic map-pattern classification using recursive partitioning and Principal Component Analysis. *Monthly Weather Review*, *130*(5), 1187–1206.

Curry, J. A., Schramm, J. L., & Ebert, E. E. (1995). Sea ice-albedo feedback mechanism. *Journal of Climate*, *8*, 240–247.

Dahni, R. R., & Ebert, E. E. 1998. *Automated Objective Synoptic Typing to Characterize Errors in NWP Model QPFs*, J31-J34, 12th Conference on Numerical Weather Prediction, Phoenix, Arizona, 11–16/1/98.

Else, B. G. T., Papakyriakou, T. N., Galley, R. J., Drennan, W. M., Miller, L. A., & Thomas, H. (2011). Wintertime CO_2 fluxes in an Arctic polynya using eddy covariance: Evidence for enhanced air–sea gas transfer during ice formation. *Journal of Geophysical Research*, *116*, C00G03. doi:10.1029/2010JC006760

Frakes, B., & Yarnal, B. (1997). A procedure for blending manual and correlation-based synoptic classifications. *International Journal of Climatology*, *17*, 1381–1396. doi:10.1002/(SICI)1097-0088(19971115)17:13<1381::AID-JOC204>3.0.CO;2-Q

Francis, J. A., & Vavrus, S. J. (2012). Evidence linking Arctic amplification to extreme weather in mid-latitudes. *Geophysical Research Letters*, *39*, L06801. doi:10.1029/2012GL051000

Galley, R. J., Else, B. G. T., Prinsenberg, S. J., & Barber, D. G. (2013). Sea ice concentration, extent, age, motion and thickness in regions of proposed offshore oil and gas development near the Mackenzie Delta, Canadian Beaufort Sea. *Arctic*, *66*(1), 105–116.

Guest, P. S., Glendening, J. W., & Davidson, K. L. (1995). An observation and numerical study of wind stress variations within marginal ice zones. *Journal of Geophysical Research*, *100*(C6), 10887–10904.

Hebbinghaus, H., Schlunzen, H., & Dierer, S. (2007). Sensitivity studies on vortex development over a polynya. *Theoretical and Applied Climatology*, *88*, 1–16.

Hudak, D. R., & Young, J. M. C. (2002). Storm climatology of the southern Beaufort Sea. *Atmosphere-Ocean 40*(2), 145–158.

Kalnay, E., Kanamitsu, M., Kistler, R., Collins, W., Deaven, D., Gandin, L., … Joseph, D. (1996). The NCEP/NCAR 40-year reanalysis project. *Bulletin of the American Meteorological Society*, *77*, 437–471.

Key, J., & Crane, R. G. (1986). A comparison of synoptic classification schemes based on "objective" procedures. *Journal of Climatology*, *6*, 375–388.

Kidson, J. (1994). An automated procedure for the identification of synoptic types applied to the New Zealand region. *International Journal of Climatology*, *14*, 711–721.

Kidson, J. (1995). A synoptic climatological evaluation of the changes in the CSIRO nine-level model with doubled CO_2 in the New Zealand region. *International Journal of Climatology*, *15*, 1179–1194.

Kirchhofer, W. (1974). Classification of European 500 mb patterns. *Arbeitsbericht der Schweizerischen Meteorologischen Zentralan-stalt*, Vol. 43, Zurich.

Kohonen, T. (1990). The self-organizing map. *Proceedings of IEEE*, *78*, 1464–1480.

Kwok, R., Cunningham, G. F., Wensnahan, M., Rigor, I., Zwally, H. J., & Yi, D. (2009). Thinning and volume loss of the Arctic Ocean sea ice cover: 2003–2008. *Journal of Geophysical Research*, *114*, C07005. doi:10.1029/2009JC005312

Laxon, S. W., Giles, K. A., Ridout, A. L., Wingham, D. J., Willatt, R., Cullen, R., … Davidson, M. (2013). CryoSat-2 estimates of Arctic sea ice thickness and volume. *Geophysical Research Letters*, *40*. doi:10.1002/grl.50193

Lund, I. A. (1963). Map pattern classification by statistical methods. *Journal of Applied Meteorology*, *2*, 56–65.

Lynch, A. H., Cassano, E. N. Cassano, J. J., & Lestak, L. R. (2003). Case studies of high wind events in Barrow, Alaska: Climatological context and development processes. *Monthly Weather Review*, *131*, 719–732.

Lynch, A. H., Curry, J. A., Brunner, R. D., & Maslanik, J. A. (2004). Toward an integrated assessment of the impacts of extreme winds events on Barrow, Alaska. *Bulletin of the American Meteorological Society*, *85*, 209–221.

Markus, T., Stroeve, J. C., & Miller, J. (2009). Recent changes in Arctic sea ice melt onset, freeze-up and melt season length. *Journal of Geophysical Research*, *114*, C12024. doi:10.1029/2009/JC005436

Maslanik, J., Stroeve, J., Fowler, C., & Emery, W. (2011). Distribution and trends in Arctic sea ice age through spring 2011. *Geophysical Research Letters*, *38*, L13502. doi:10.1029/2011GL047735

Maxwell, J. B. (1980). The climate of the Canadian Arctic Islands and adjacent waters. Environment Canada, Atmospheric Environment Service, Climatological Studies number 30, Hull, QC: Minister of Supply and services Canada, ISBN 0–660–50641–6.

McKendry, I.G., Stahl, K., & Moore, R.D. (2006). Synoptic sea-level pressure patterns generated by a general circulation model: Comparison with types derived from NCEP re-analysis and implications for downscaling. *International Journal of Climatology*, *26*, 1727–1736. doi:10.1002/joc.1337

Mesinger, F., DiMego, G., Kalnay, E., Mitchell, K., Shafran, P.C., Ebisuzaki, W., … Shi, W. (2006). North American regional reanalysis. *Bulletin of the American Meteorological Society*, *87*, 343–360.

Moore, G. W. K. (2012). Decadal variability and a recent amplification of the summer Beaufort Sea High. *Geophysical Research Letters*, *39*, L10807. doi:10.1029/2012GL051570

Moore, G. W. K., & Pickart, R. S. (2012). The Wrangel Island Polynya in early summer: Trends and relationships to other polynyas and the Beaufort Sea High. *Geophysical Research Letters*, *39*, L05503. doi:10.1029/2011GL050691

Ogi, M., Yamazaki, K., & Wallace, J. (2010). Influence of winter and summer surface wind anomalies on summer Arctic sea ice extent. *Geophysical Research Letters*, *37*, L07701. doi:10.1029/2009GL042356

Ogi, M., & Wallace, J. M. (2012). The role of summer surface wind anomalies in the summer Arctic sea ice extent in 2010 and 2011. *Geophysical Research Letters*, *39*, L09704. doi:10.1029/2012GL051330

Overland, J. E. (2009). Meteorology of the Beaufort Sea. *Journal of Geophysical Research*, *114*, C00A07. doi:10.1029/2008JC004861

Overland, J. E., & Wang, M. (2013). When will the summer Arctic be nearly sea ice free? *Geophysical Research Letters*, *40*, 2097–2101. doi:10.1002/grl.50316

Perovich, D. K., Richter-Menge, J. A., Jones, K. F., & Light, B. (2008). Sunlight, water, and ice: Extreme Arctic sea ice melt during the summer of 2007. *Geophysical Research Letters*, *35*, L11501. doi:10.1029/2008GL034007

Pickart, R. S., Moore, G. W. K., Torres, D. J., Fratantoni, P. S., Goldsmith, R. A., & Yang, J. (2009). Upwelling on the continental slope of the Alaskan Beaufort Sea: Storms, ice, and oceanographic response. *Journal of Geophysical Research*, *114*, C00A13. doi:10.1029/2008JC005009

Rampal, P., Weiss, J., & Marsan, D. (2009). Positive trend in the mean speed and deformation rate of Arctic sea ice, 1979–2007. *Journal of Geophysical Research*, *114*, C05013. doi:10.1029/2008JC005066

Rothrock, D. A., & Thorndike, A. S. (1984). Measuring the sea ice floe distribution. *Journal of Geophysical Research*, *89*(C4), 6477–6486.

Rothrock, D. A., Yu, Y., & Maykut, G. A. (1999). Thinning of the Arctic sea-ice cover. *Geophysical Research Letters*, *26*(23), 3469–3472.

Screen, J. A., Simmonds, I., & Keay, K. (2011). Dramatic inter-annual changes of perennial Arctic sea ice linked to abnormal summer storm activity. *Journal of Geophysical Research*, *116*, D15105. doi:10.1029/JD015847

Sepp, M., & Jaagus, J. (2011). Changes in the activity and tracks of Arctic cyclones. *Climatic Change*, *105*, 577–595. doi:10.1007/s10584-010-9893-7

Serreze, M. C., & Barry, R. G. (2005). *The Arctic climate system*. Cambridge: Cambridge University Press.

Serreze, M. C., & Barrett, A. P. (2007). The summer cyclone maximum over the central Arctic Ocean. *Journal of Climate*, *21*, 1048–1065.

Serreze, M. C. (2009). *Northern hemisphere cyclone locations and characteristics from NCEP/NCAR reanalysis data*. Boulder, Colorado, USA: National Snow and Ice Data Center. Retrieved from http://nsidc.org/data/docs/daac/nsidc0423_cyclone/#access_tools

Simmonds, I., & Keay, K. (2009). Extraordinary September Arctic sea ice reductions and their relationships with storm behavior over 1979–2008. *Geophysical Research Letters*, *36*, L19715. doi:10.1029/2009GL039810

Small, D., Atallah, E., & Gyakum, J. (2011). Wind regimes along the Beaufort Sea coast favorable for strong wind events at Tuktoyaktuk. *Journal of Applied Meteorology and Climatology*, *50*, 1291–1306.

Sorteberg, A., & Walsh, J. E. (2008). Seasonal cyclone variability at 70°N and its impact on moisture transport into the Arctic. *Tellus*, *60A*, 570–586.

Spreen, G., Kwok, R., & Menemenlis, D. (2011). Trends in Arctic sea ice drift and role of wind forcing: 1992–2009. *Geophysical Research Letters*, *38*, L19501. doi:10.1029/2011GL048970

Squire, V. A., Vaughan, G. L., & Bennetts, I. G. (2009). Ocean surface wave evolvement in the Arctic basin. *Geophysical Research Letters*, *36*, L22502. doi:10.1029/2009GL040676

Stahl, K., Moore, R. D., & McKendry, I. G. (2006a). The role of synoptic-scale circulation in the linkage between large-scale ocean-atmosphere indices and winter surface climate in BC, Canada. *International Journal of Climatology*, *26*, 541–560.

Stahl, K., Moore, R. D., & McKendry, I. G. (2006b). Climatology of winter cold spells in British Columbia, Canada, in relation to mountain pine beetle outbreaks. *Climate Research*, *32*, 13–23.

Steele, M. (1992). Sea ice melting and floe geometry in a simple ice-ocean model. *Journal of Geophysical Research*, *97*(C11), 17,729–17,738. doi:10.1029/92JC01755

Stegall, S., & Zhang, J. (2012). Wind field climatology, changes, and extremes in the Chukchi-Beaufort seas and Alaska North Slope during 1979–2009. *Journal of Climate*, *25*(3), 8075–8089.

Stroeve, J. C., Serreze, M. C., Holland, M. M., Kay, J. E., Maslanik, J., & Barrett, A. P. (2011). The Arctic's rapidly shrinking sea ice cover: A research synthesis. *Climate Change*, *110*(3–4), 1005–1027. doi:10.1007/s10584-011-0101-1

Stroeve, J. C., Markus, T., Boisvert, L., Miller, J., & Barrett, A. (2014). Changes in Arctic melt season and implications for sea ice loss. *Geophysical Research Letters*, *41*, 1216–1225. doi:10.1002/2013GL058951

Tang, Q., Zhang, X., & Francis, J. A. (2013). Extreme summer weather in northern mid-latitudes linked to a vanishing cryosphere. *Nature Climate Change*, doi:10.1038/NCLIMATE2065

Vavrus, S. J. (2013). Extreme Arctic cyclones in CMIP5 historical simulations. *Geophysical Research Letters*, *40*, 6208–6212. doi:10.1002/2013GL058161

Vincent, L. A., Wang, X. L., Milewska, E. J., Wan, H., Yang, F., & Swail, V. (2012). A second generation of homogenized Canadian monthly surface air temperature for climate trend analysis. *Journal of Geophysical Research*, *117*, D18110. doi:10.1029/2012JD017859

Wadhams, P., Gill, A. E., & Linden, P. F. (1979). Transects by submarine of the East Greenland Polar front. *Deep Sea Research Part A. Oceanographic Research Papers*, *26A*, 1311–1327.

Wadhams, P., Squire, V. A., Goodman, D. J., Cowan, A. M., & Moore, S. C. (1988). The attenuation of ocean waves in the marginal ice zone. *Journal of Geophysical Research*, *93*, 6799–6818. doi:10.1029/JC093iC06p06799

Wang, J., Zhang, J., Watanabe, E., Ikeda, M., Mizobata, K., Walsh, J. E., Bai, X., & Wu, B. (2009). Is the Dipole Anomaly a major driver to record lows in Arctic summer sea ice extent? *Geophysical Research Letters 36*, L05706. doi:10.1029/2008GL036706

Wu, B., Wang, J., & Walsh, J. E. (2006). Dipole anomaly in the winter Arctic atmosphere and its association with Arctic sea ice motion. *Journal of Climate*, *19*(2), 210–225. doi:10.1175/JCLI3619.1

Yarnal, B. (1985). A 500 mb synoptic climatology of Pacific north-west coast winters in relation to climatic variability. *Journal of Climatology*, *5*, 237–252.

Yarnal, B. (1993). *Synoptic climatology in environmental analysis: A primer*. London: Belhaven Press.

Zhang, X., Walsh, J. E., Zhang, J., Bhatt, U. S., & Ikeda, M. S. (2004). Climatology and interannual variability of Arctic cyclone activity: 1948–2002. *Journal of Climatology*, *17*, 2300–2317.